Engineering Biomimetic Gelatin Based Nanostructures as Synthetic Substrates for Cell Culture

Shaleena K. Pazhanimala, Driton Vllasaliu[ID] and Bahijja T. Raimi-Abraham *[ID]

School of Cancer and Pharmaceutical Sciences, King's College London, London SE1 9NH, UK;
shaleena.koomullukkad_pazhanimala@kcl.ac.uk (S.K.P.); driton.vllasaliu@kcl.ac.uk (D.V.)
* Correspondence: Bahijja.Raimi-Abraham@kcl.ac.uk; Tel.: +44-207-848-0622

check for updates

Abstract: There is a need for synthetic substrates that replicate the natural environment for in vitro intestinal models. Electrospinning is one of the most versatile and cost-effective techniques to produce nanofibrous scaffolds mimicking the basement membrane topography. In this study, three different novel electrospun nanofibrous scaffolds made of a polycaprolactone (PCL), gelatin, and poloxamer 188 (P188) blend were produced and compared with PCL and PCL/gelatin fibers produced using the same solvent system and electrospinning parameters. Each polymer solution used in this experiment was electrospun at four different voltages to study its influence on fiber diameter. The morphology and physical characteristics of the fibers were studied using scanning electron microscopy and atomic force microscopy. The average fiber diameter of all scaffolds was within 200–600 nm and no significant decrease in diameter with an increase in voltage was observed. Attenuated total reflection Fourier transform infrared spectroscopy was used to determine the chemical characteristics of the nanofibrous scaffold. The conductivity of the polymer solutions was also analyzed. Biocompatibility of the scaffolds was determined by a cell proliferation study performed using colorectal carcinoma (Caco-2) cells. PCL/gelatin/P188 scaffolds exhibited higher cell proliferation compared to PCL, PCL/gelatin scaffolds, and the control (tissue culture multi-well plate) with PCL/gelatin/P188 80:10:10 sample showing the highest cell proliferation.

Keywords: electrospinning; polycaprolactone (PCL); gelatin; nanofibers; P188

1. Introduction

The basement membrane (BM) is a specialized form of the extracellular matrix (ECM) present directly under the basal surface of epithelial and endothelial tissues of eumetazoans, where it supports and interacts with other components of the ECM and epithelial cells to promote cell proliferation, migration, and differentiation [1–3].

Although the BM is known to possess some barrier functionality (to cell and macromolecular migration), it is a relatively porous (pore size ~10–130 nm [2]) nanofibrous network mainly composed of a self-polymerizing network of collagen IV and laminin which are connected to one another by glycoproteins, namely nidogen and heparin sulphate proteoglycan [1,2,4,5]. The structure, thickness, and composition of the BM differ with location and tissue type, healthy ageing, and disease [1,2,6,7]. With respect to the latter, examples include asthma and collagenous colitis—a type of nonspecific inflammatory bowel disease which results in an increase of subepithelial BM thickness [8,9].

In the field of drug delivery, while the drug barrier functions of mucus and epithelium are relatively well-characterized, the filter function of the BM is seldom studied [10–12]. But currently, there is a growing interest to understand the barrier function of the BM due to advances in the mucosal

delivery of complex therapeutics such as macromolecules and nanomedicines [12,13]. The diffusion of macromolecules through the BM of non-keratinized oral mucosal epithelium was initially studied by Alfano et al., who observed that the BM restricts the penetration of smaller macromolecules (inulin, 5 kDa), while allowing easy passage of larger macromolecules (Dextran, 20 kDa) [14]. This restriction of smaller macromolecules in this study was considered as the result of adhesion or penetration of inulin at the crevices of BM structural proteins [14]. Recently, a similar study was performed by Vllasaliu et al. who observed that decellularized BM synthesized by airway epithelial cells restricts the diffusion of macromolecules in a size-dependent manner [12].

There is a need for a well-characterized biomimetic BM substitute which could efficiently replicate the native BM for research in the areas of tissue engineering and drug delivery [15–18]. Our study focused on the biomimicry of intestinal epithelial BM due to its relevance in drug and nutrient absorption/delivery studies, investigations on intestinal diseases, and infection studies [15–18]. These studies currently commonly utilize the Caco-2 cell model [14–17]. This model lacks a proper BM and therefore fails to replicate the complex substrate nanoenvironment taking into account the size, geometry, roughness, stiffness, porosity, and macromolecular composition of the BM [12,19,20]. Naturally derived matrices exist, which consist of BM extracts (Matrigel: BM extract secreted by Engelbrecht-Holm-Swarm mouse sarcoma cells) and purified BM proteins (Laminin 111, fibrin gels and hyaluronic acid gels); however, these systems have shown to be unreliable due to their tumor derived nature (which restricts its use in clinical translational studies), lot-to-lot variation, and the inability to understand and decouple their mechanical and biochemical properties [21]. For example, a change in mechanical properties such as matrix density resulted in a change in biochemical properties, such as fiber density and structure, making it impossible to alter one property without disturbing the other [21]. As a result, there is a growing interest and need to fabricate synthetic substrates or BM mimetics with features and properties of human native BMs, as well as easily tunable bioactivity and mechanical properties [12,21].

Electrospinning is a well-known versatile, cost-effective, and commonly used nanofabrication method which can be easily upgraded for industrial-scale production of nanofibers [22]. Electrospinning involves the use of a high voltage that repels the surface tension of the polymer solution droplet pumped through a needle [22]. Once the electric charge on the surface of the droplet overcomes the surface tension, a jet of nanofibers is formed and collected [23]. Different synthetic and natural polymers can be used to produce the nanofibers [23]. The physical and chemical properties of these polymers, along with the nanoscale nature of the electrospun fibers are considered to have a profound influence on the cell-scaffold interaction and cell behavior [24]. For instance, previous studies have demonstrated an increase in cell adhesion, cell differentiation with an increase in polymer hydrophilicity, charge density, roughness at the nanoscale, and stiffness with variation in the scaffold porosity [25–31]. As there is no ideal polymer that possesses all the desired characteristics for use as a scaffold, a mixture of polymers or additives, such as cell growth promoters, can be used to tailor the characteristics to the desired scaffold [32]. In this study, two polymers (polycaprolactone (PCL), gelatin) and a non-ionic surfactant (poloxamer 188) were combined to produce an electrospun composite scaffold as a substrate for intestinal epithelial cells that could mimic the BM.

Polycaprolactone (PCL) is a non-toxic synthetic polymer with desirable mechanical characteristics, such as a slow degradation rate and higher elastic modulus, which can efficiently replicate the nanofibrous nature of the ECM when electrospun [33–36]. However, its hydrophobic nature and lack of cell recognition sites can restrict cell adhesion and overall growth [33–36]. Gelatin is a biocompatible, biodegradable, non-immunogenic natural polymer with low mechanical strength, which has inbuilt signals (arginine-glycine-aspartic acid sequence) to promote efficient cell adhesion and growth [37]. When combined with PCL, gelatin composite nanofibrous scaffolds exhibit good cell adhesion property along with good mechanical strength enabling improved cell growth [32,37]. Poloxamer 188 (P188) is a non-ionic surfactant of 8400 Da molecular weight, which has the ability to revive mammalian cells exposed to mechanical and chemical stress [38]. P188 is composed of one unit of hydrophobic

poly(oxypropylene) (POP) and two units of hydrophilic poly(oxyethylene) (POE) arranged as a triblock structure POE-POP-POE [38]. The use of P188 in culture media has shown to increase the viability and proliferation of Caco-2 cells [38]. It was reported that P188 has the capability to reseal damaged cell membranes and increase its stiffness, in turn supporting the cell to efficiently adhere to a growth support, resulting in an increase in cell adhesion and proliferation [38]. However, no cell viability studies have been conducted to understand the significance of P188 in polymer blend nanofibers and influence on cell viability [39,40]. In this study, polycaprolactone (PCL), gelatin, and poloxamer 188 composite nanofibrous scaffolds were generated using electrospinning to produce a scaffold that could act as a substrate, possibly by efficiently mimicking the epithelial BM, and have the desired mechanical and chemical properties for effective cell growth. In a previous work, Denis et al. successfully co-electrospun PCL with gelatin using low toxicity and cost-effective solvents, formic acid and acetic acid [41]. In this experiment, poloxamer 188 was incorporated into the PCL/gelatin blend scaffold to enhance the viability and proliferation of cells.

2. Materials and Methods

2.1. Materials

Polycaprolactone (PCL, Mn = 80,000 g/mol) was purchased from Sigma-Aldrich, UK. Gelatin from the porcine skin in powder form (Type A, gel strength = 300) and P188 solid (Kolliphor® P188 = Lutrol F68) were purchased from Sigma-Aldrich (Poole, UK). The solvent system includes acetic acid (≥99% pure), which was obtained from Honeywell research chemicals and formic acid (98–100% pure) was purchased from Sigma-Aldrich (Poole, UK). All were used without further purification.

2.2. Preparation of Solutions

Five polymer solutions (solvent system of acetic acid and formic acid in 90:10 %v/v concentration) with a total polymer concentration of 15% were prepared as shown in Table 1. Formic acid is known to increase the permittivity of the solvent system due to its high dielectric constant (57.2εo at 25 °C) in comparison with acetic acid (6.6εo at 25 °C) [41]. The 90% acetic acid used in the solvent mix has the ability to reduce the degradation of gelatin by formic acid [41]. The polymer solutions were prepared at room temperature by continuous stirring on a magnetic spinner for around 24 h until they are completely dissolved.

Table 1. Different polymer solutions prepared along with the concentration of each component (in %w/v) used to prepare the polymer solutions.

Polymer Solution with 90%/10% Acetic Acid Formic Acid Solvent System	The Concentration of Each Component in the Total Polymer Concentration of 15% (w/v)		
	PCL	Gelatin	Poloxamer 188
PCL	100%	-	-
PCL/gelatin (90:10)	90%	10%	-
PCL/gelatin/P188 (85:10:5)	85%	10%	5%
PCL/gelatin/P188 (80:10:10)	80%	10%	10%
PCL/gelatin/P188 (70:10:20)	70%	10%	20%

For electrospinning process, the syringe with the solution was mounted on to a syringe pump (Intertek, Cole Palmer® , Vernon Hills, IL, USA), which was arranged vertically at a distance of 10 cm from the grounded collector covered with aluminum foil. The negative electrode from the high voltage power supply was clamped to the collector and the positive electrode was clamped to the needle. The polymer solutions loaded into a 5 mL syringe (BD Plastipak) and attached to a 21-gauge (inner diameter = 0.02 inch, outer diameter = 0.032 inch) needle (FINE-JECT®) were electrospun at four different voltages (18 kV, 20 kV, 22 kV, and 24 kV). The syringe pump was set to maintain the flow rate

of the solution at 0.5 mL/h throughout the electrospinning process. All the electrospinning experiments were performed at an ambient temperature of 20–22 °C and humidity of 40–50%.

2.3. Scanning Electron Microscopy Studies

The surface morphology of the electrospun fibrous membrane was examined by scanning electron microscopy (SEM) using a HITACHI S4000 instrument (Hitachi, Tokyo, Japan). A total of 10 nm gold-coated samples, attached to a 12 mm carbon adhesive disc was scanned at different magnifications (400 to 10,000 times) to determine the morphology of the fibers. Images were analyzed using ImageJ digital analysis software to measure the diameters of the individual fibers. A total of 100 measurements was taken and used to obtain the average fiber diameter. A fiber diameter distribution histogram was plotted using Microsoft Excel 2016.

2.4. Atomic Force Microscopy Studies

The topography and roughness of the fibrous scaffolds electrospun at 22 kV were evaluated by a Bruker Dimension Icon Atomic Force Microscopy instrument with Scan Analyst. The samples fixed onto a specimen disc (SPM-15 mm Agar Scientific) were scanned using peak force tapping mode at a rate of 0.75 Hz. The antimony doped Si probe (RTESPA-300 BRUKER model) was used, which has a spring constant of 40 N/m.

2.5. Attenuated Total Reflection Fourier Transform Infrared Spectroscopy (ATR-FTIR) Studies

Fourier transform infrared spectroscopy (FTIR–PerkinElmer Frontier) was performed on the composite scaffolds to determine the presence of PCL, gelatin, and P188. The spectra were collected using an attenuated total reflection (ATR) mode from 4000 to 600 cm^{-1} using 4 scans per sample.

2.6. Cell Viability Studies

Five nanofibrous scaffolds electrospun at 22 kV were separated from the aluminum foil and cut to fit the 12 well plates. Scaffolds were sterilized by exposing to UV light (CL-1000 Ultraviolet Crosslinker) for 10 min. Human Caco-2 (colorectal carcinoma, obtained from European Collection of Authenticated Cell Cultures) cells were seeded onto a scaffold at 2×10^5 cells/well and cultured in Dulbecco's Modified Eagle Medium (DMEM; purchased from Sigma-Aldrich, Poole, UK), supplemented with glucose, non-essential amino acids, 10% foetal bovine serum, and 1% antibiotic/antimycotic solution (penicillin, streptomycin, and amphotericin). Cells were also seeded on to empty culture wells for comparison. Alamar Blue assay was performed on day 2 and day 4 to determine the change in cell growth. This assay includes an oxidation and reduction indicator (Alamar Blue® reagent–ThermoFisher Scientific, Waltham, MA, USA), which can indicate the reduction of growth medium due to cell proliferation by changing color or by fluorescence [42]. The reagent was added to each of the wells and incubated at 37 °C for 1 h, and the fluorescence intensity of 100 µL of the reagent was measured using the CytoFluor® multiwell plate reader.

2.7. Statistical Analysis

The experimental mean values obtained for conductivity, fiber diameter, and roughness of the fibers are expressed in mean ± standard deviation. Cell metabolic activity is presented as % fluorescence compared to control (cells cultured on tissue culture multiwell plate plastic). The statistical significance of change of the nanofiber diameter with the change in voltage was evaluated using analysis of variance (ANOVA) using R software. Statistical significance cutoff at $p < 0.05$ was used; *, ** and *** denote $p < 0.05$, $p < 0.01$, and $p < 0.001$, respectively.

3. Results

3.1. Morphology of PCL/Gelatin/Poloxamer 188 (P188) Scaffolds in Comparison with PCL/Gelatin and PCL Nanofibers

SEM images and diameter distribution of PCL and PCL/gelatin (90:10) composites are shown in Figure 1, Figure 2 and Table 2, respectively. Figures 3–5, on the other hand, represents SEM images and diameter distribution of three different samples of PCL/gelatin/P188 with a concentration ratio of 85:10:5, 80:10:10, and 70:10:20 respectively.

Table 2 shows the average diameter along with the standard deviation of all the five samples electrospun at four different voltages (18 kV, 20 kV, 22 kV, and 24 kV) obtained using ImageJ analysis of ×10,000 magnified samples. It can be seen that the average diameter of all the fibrous samples is in the nanometer range. Moreover, it was observed that the scaffolds not only had fibers of varying diameter, but the diameter of the individual fibers vary along its length. Beads were also observed in all composite nanofibrous scaffolds.

To determine the nanotopography of the scaffold, the nanofibers were further characterized using AFM. The topographic variation with the change in the composition of the fibers can be clearly observed in the AFM images (Figure 6). The mean roughness value (Ra) of scaffolds was also obtained from the AFM images. The roughness average (Ra) is an arithmetic mean value of individual height measurements obtained using AFM of peaks and valleys on the surface of the scaffold [43]. Ra value is directly proportional to roughness [43].
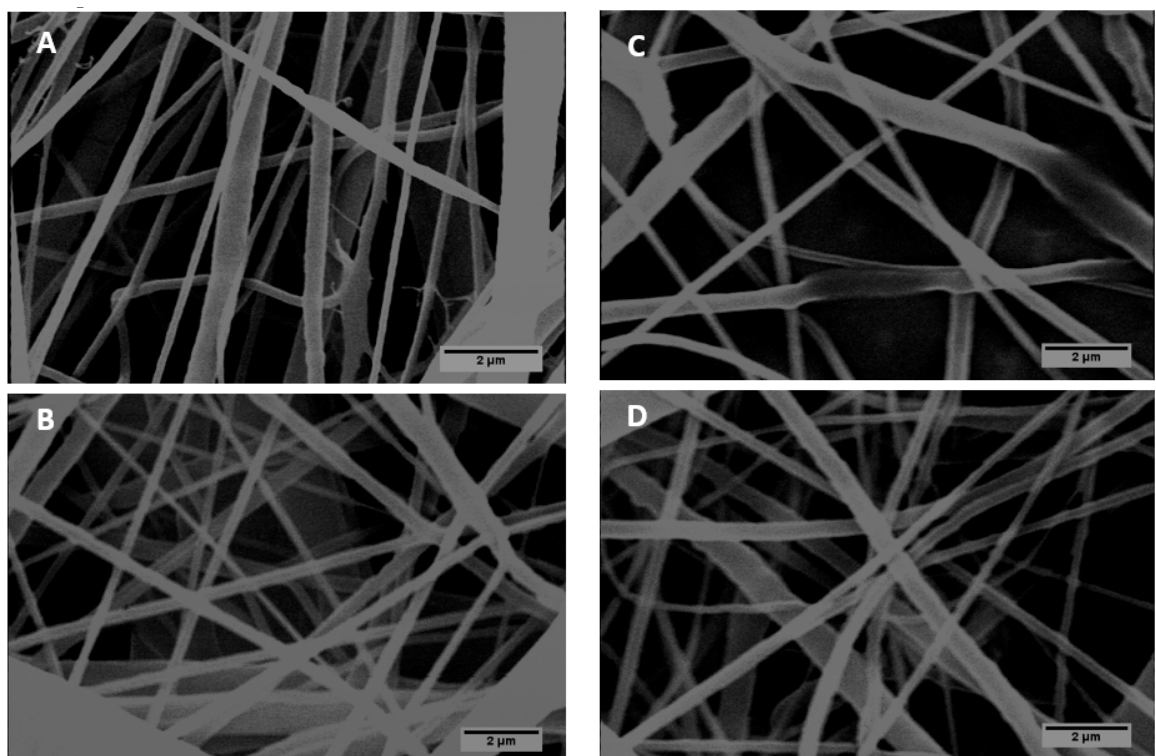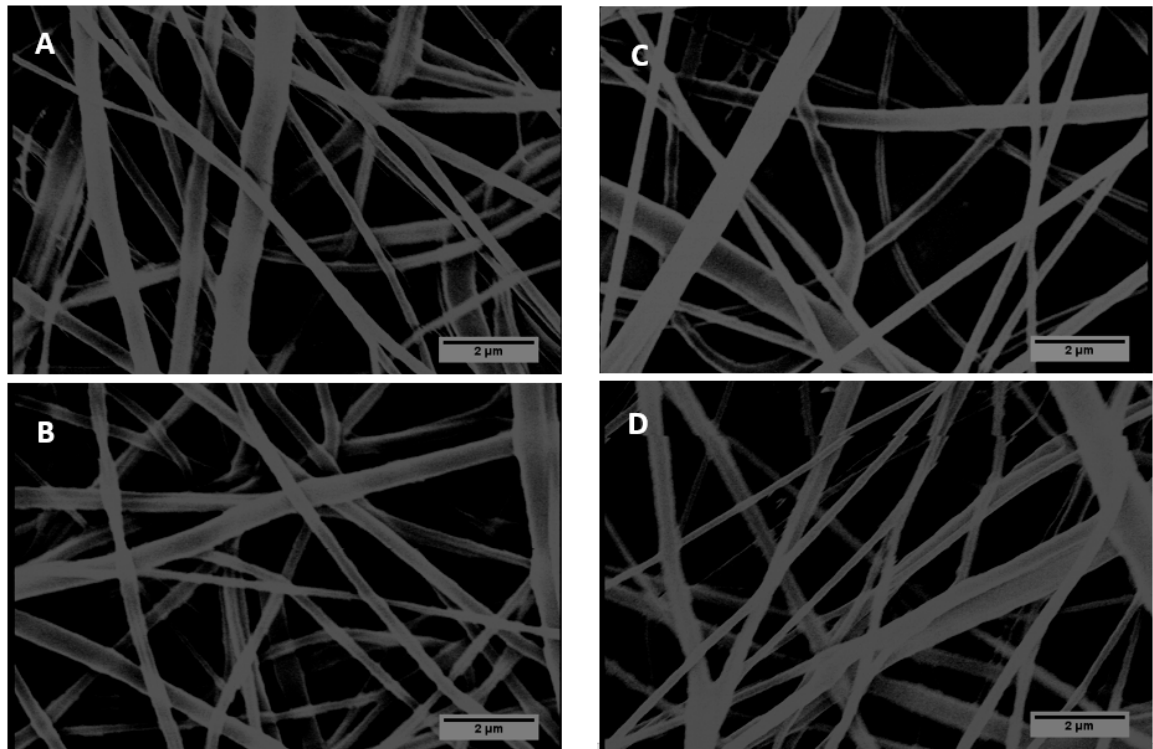

Figure 1. SEM images of the polycaprolactone (PCL) nanofibers electrospun at (**A**) 18 kV, (**B**) 20 kV, (**C**) 22 kV, and (**D**) 24 kV voltages. The images were measured at a magnification of ×8000 to ×10,000.
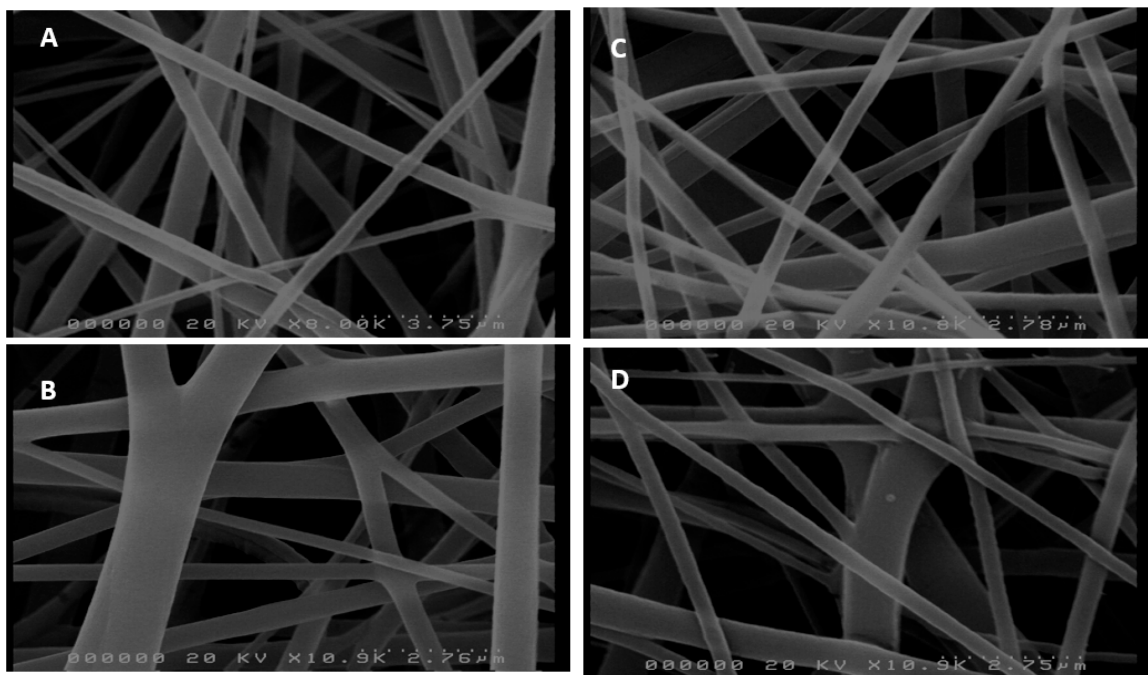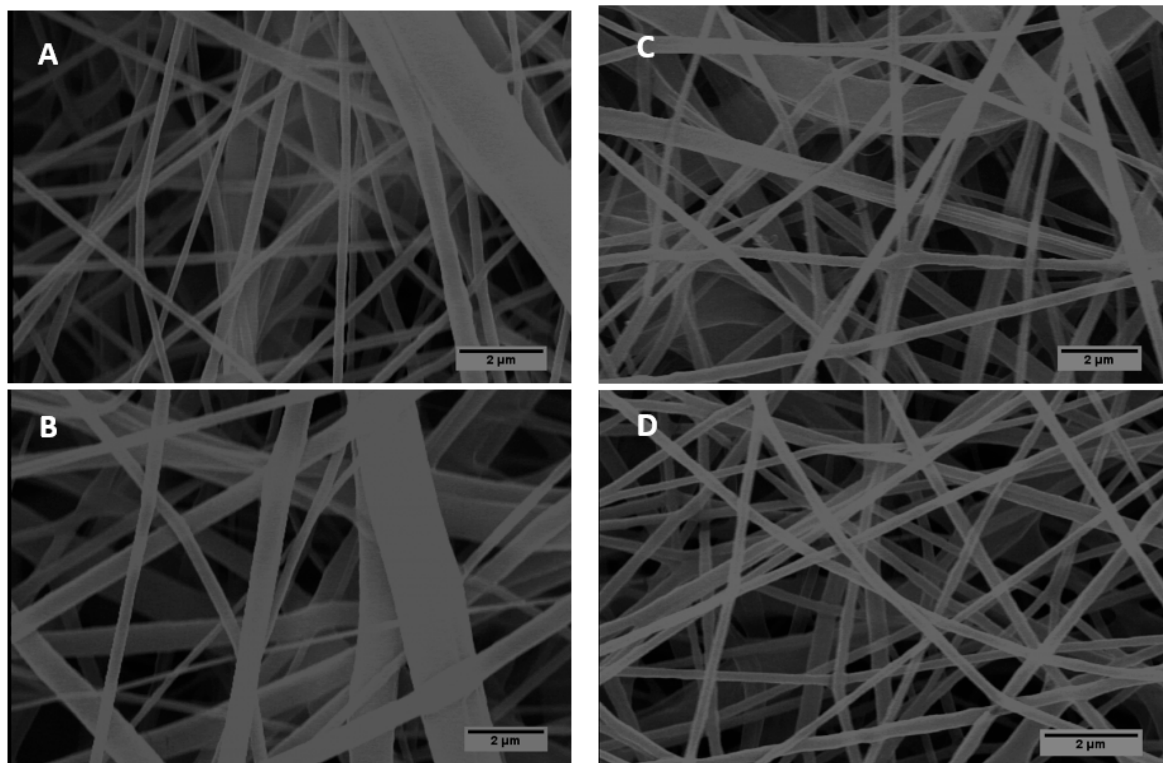
Figure 2. SEM images of the PCL/gelatin (90:10 %w/v) composite nanofibers electrospun at (**A**) 18 kV, (**B**) 20 kV, (**C**) 22 kV, and (**D**) 24 kV voltages. The images were measured at a magnification of ×8000 to ×10,000.
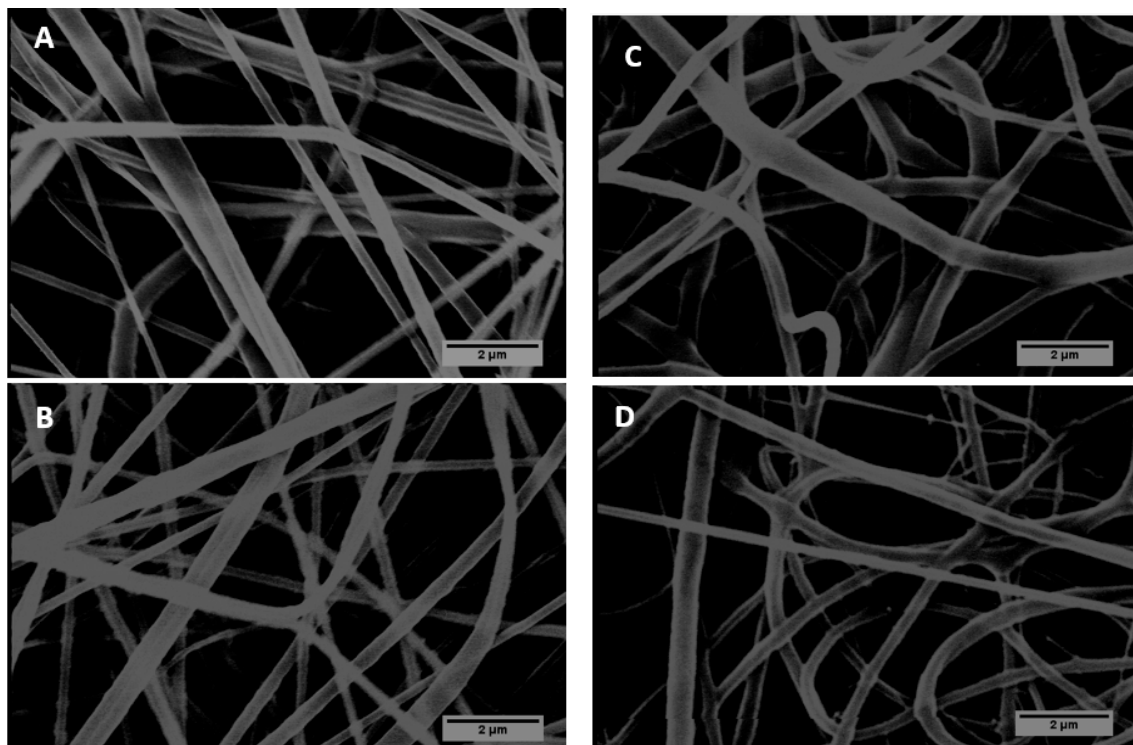
Figure 3. SEM images of the PCL/gelatin/P188 (85:10:5 %w/v) composite nanofibers electrospun at (**A**) 18 kV, (**B**) 20 kV, (**C**) 22 kV, and (**D**) 24 kV voltages. The images were measured at a magnification of ×9000 to ×10,000.

Figure 4. SEM images of the PCL/gelatin/188 (80:10:10 %w/v) composite nanofibers electrospun at (**A**) 18 kV, (**B**) 20 kV, (**C**) 22 kV, and (**D**) 24 kV voltages. The images were measured at a magnification of ×9000 to ×10,000.

Figure 5. SEM images of the PCL/gelatin/P188 (70:10:20 %w/v) composite nanofibers electrospun at (**A**) 18 kV, (**B**) 20 kV, (**C**) 22 kV, and (**D**) 24 kV voltages. The images were measured at a magnification of ×8000 to ×10,000.

Table 2. The average fiber diameter (n = 100) of the five different fibrous scaffolds along with their standard deviation.

|	Average Fiber Diameter (nm) of Fibers Electrospun at			
Samples	**18 kV**	**20 kV**	**22 kV**	**24 kV**
PCL	383 ± 301	425 ± 419	453 ± 314	487 ± 302
PCL/Gelatin (90:10)	307 ± 109	595 ± 340	282 ± 190	384 ± 245
PCL/ Gelatin/ P188 (85:10:5)	280 ±126	297 ± 181	390 ± 158	291 ± 109
PCL/ Gelatin/ P188 (80:10:10)	361 ± 175	337 ± 129	327 ± 196	239 ± 107
PCL/ Gelatin/ P188 (70:10:20)	363 ± 336	463 ± 317	306 ± 163	227 ± 62
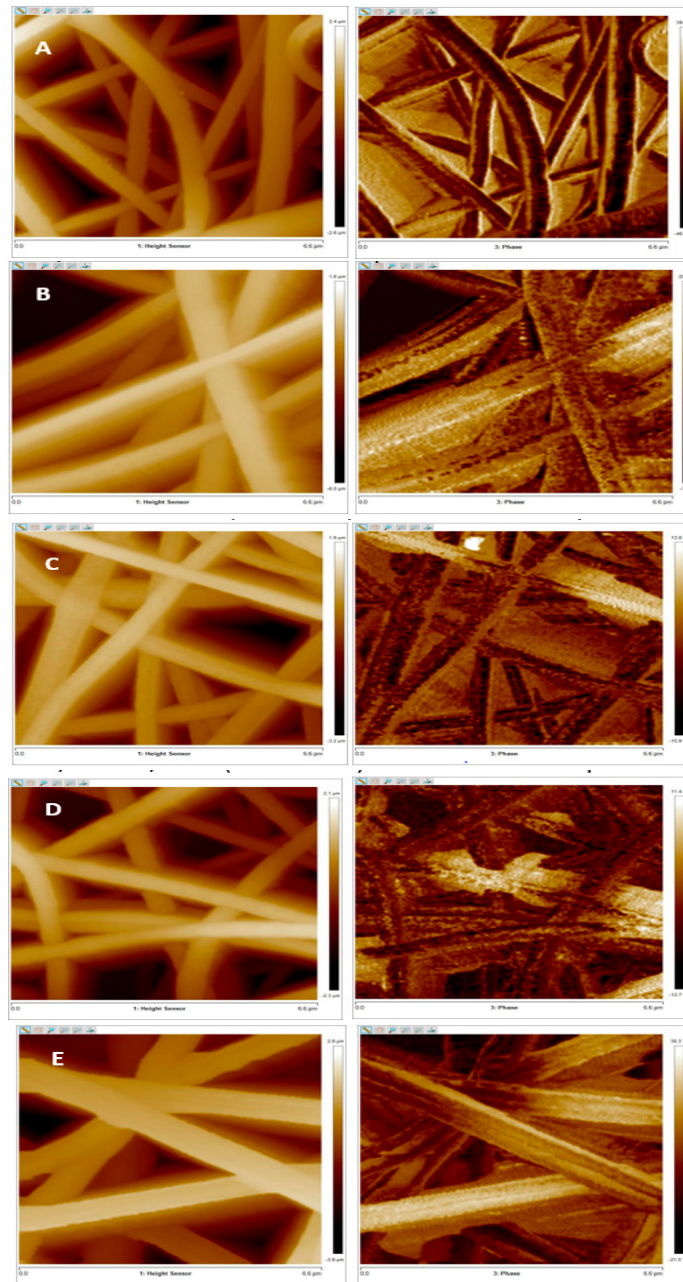
Figure 6. The height and phase AFM images of (**A**) PCL, (**B**) PCL/gelatin, (**C**) PCL/gelatin/P188 of concentration 85:10:5 %w/v, (**D**) PCL/gelatin/P188 of concentration 80:10:10 %w/v, and (**E**) PCL/gelatin/P188 of concentration 70:10:20 %w/v electrospun at 22 kV along with the (the scanning area was 6.6 μm to 6.6 μm).

3.2. Chemical Characteristics of the Scaffolds to Determine the Presence of P188 and Gelatin in the Composites

Figure 7A shows the ATR-FTIR analysis of PCL and PCL/gelatin fibrous scaffolds in comparison with the PCL and gelatin raw materials. The spectrum obtained for PCL nanofibrous scaffolds was almost identical to the one obtained for pure PCL raw material. Both have the characteristic asymmetric CH2 stretching at ~2944 cm^{-1}, symmetric CH2 stretching at ~2867 cm^{-1}, carbonyl (C = O) stretching at ~1293 cm^{-1}, and C–H and C–O stretching at ~1237 cm^{-1}. All of these bands are also observed in PCL/gelatin composite fibers along with the amide I (at ~1629 cm^{-1}) and amide II (at ~1522 cm^{-1}) bands corresponding to the C = O stretching vibration and the N–H bending coupled with C–N stretching vibration of the gelatin, respectively. This confirms the presence of gelatin in the PCL/gelatin composite fibers.


(A)

(B)
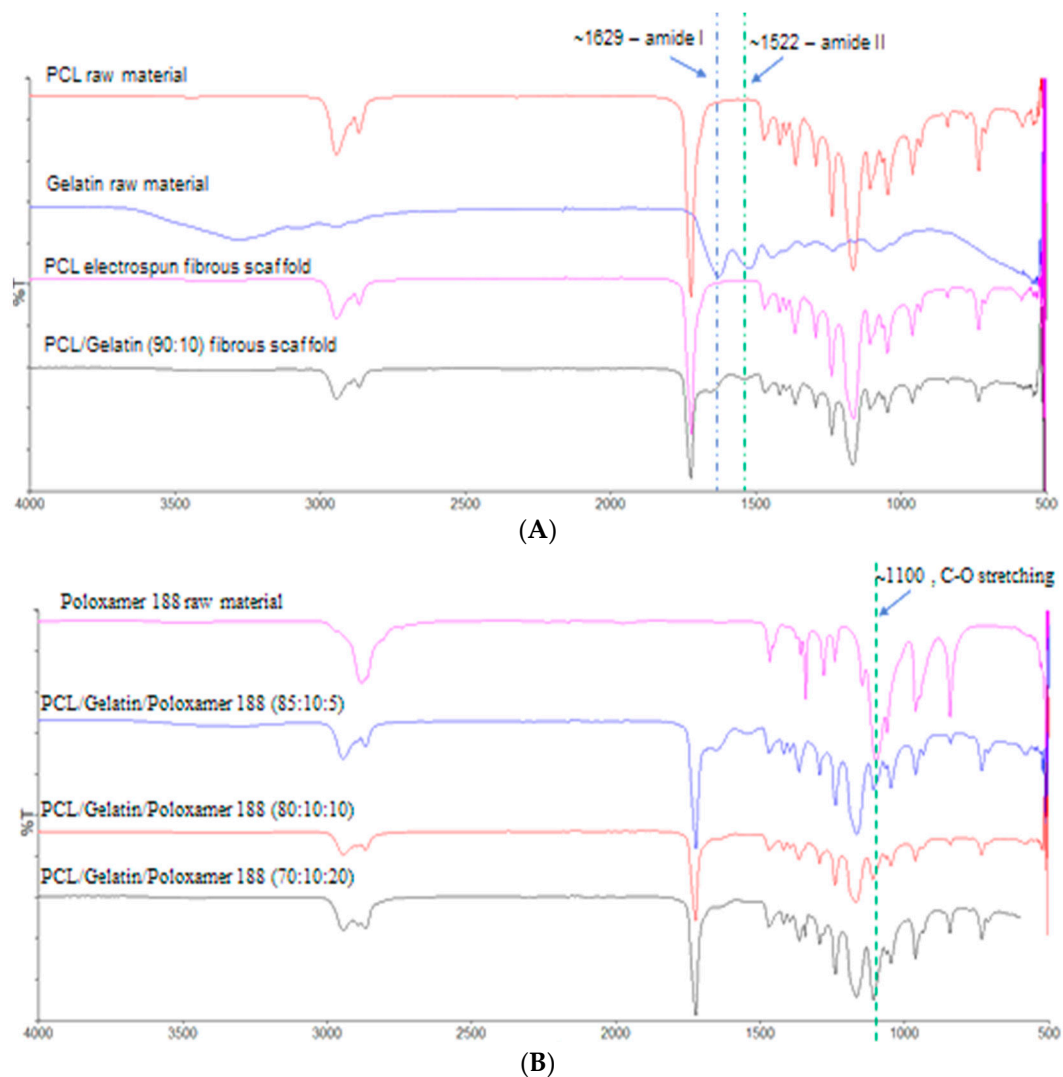
Figure 7. (**A**) Attenuated total reflection Fourier transform infrared spectroscopy (ATR-FTIR) spectra of PCL and PCL/gelatin composite electrospun nanofibers compared with the PCL and gelatin pure raw materials. (**B**) ATR-FTIR spectra of three different concentrations of PCL/Gelatin/P188 composite electrospun nanofibers compared with the pure raw material of P188 (were %T is the transmission percentage).

Figure 7B, on the other hand, shows the ATR-FTIR spectrum of all the three different samples of PCL/gelatin/P188 (85:10:5, 80:10:10, 70:10:20) compared to that of the pure P188 raw material. Three characteristic peaks exhibited by pure P188 are, the O–H stretch at ~3010 to 2800 cm^{-1}, C–H stretching

at ~2881 cm^{-1}, and C–O group stretching at ~1100 cm^{-1}. Presence of these peaks, along with the peaks corresponding to the PCL and gelatin in all the three PCL/gelatin/P188 composite samples confirms the successful blending of P188 with the PCL/gelatin to produce the substrates. Moreover, as shown in Figure 7, the intensity of the peak at ~1100cm^{-1} (C–O stretching of P188) increases with the increase in the concentration of P188, corroborating its presence in the scaffolds.

3.3. Cell Viability Studies

The biocompatibility of the biomaterial was determined by its ability to promote cell attachment and growth [39]. The cell proliferation on all the scaffolds, along with the control, increased during four days of study (Figure 8). The novel PCL/gelatin/P188 scaffolds showed the highest cell proliferation (indicated by measuring cell metabolic activity), suggesting an improved biocompatibility when compared to PCL, PCL/gelatin. Cell proliferation on these substrates was also higher than the control (Figure 8).
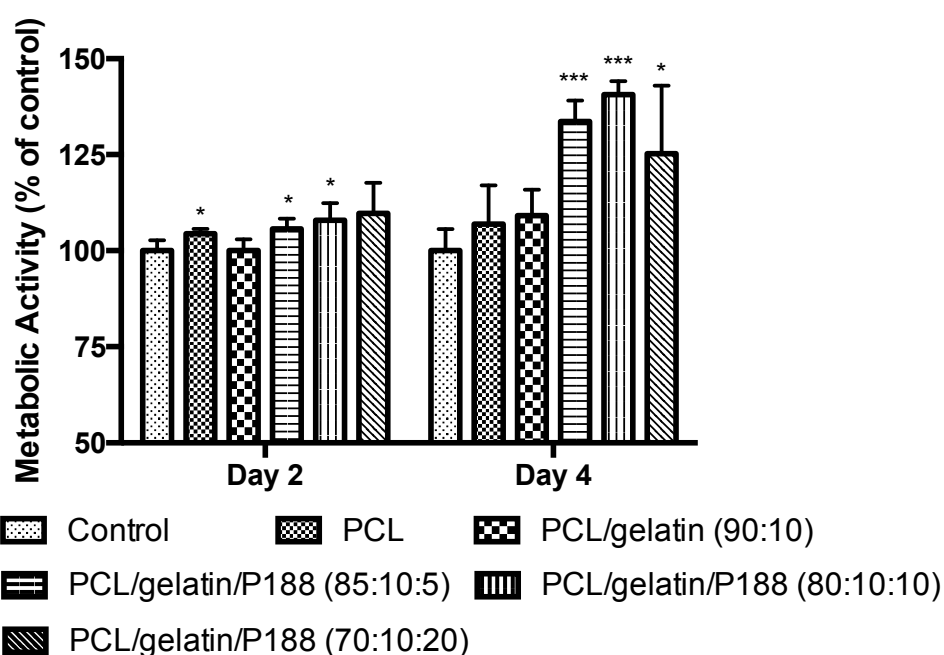
Figure 8. The mean fluorescence indicating the Caco-2 cell viability when cultured on three different PCL/gelatin/P188 (concentration ratios of 85:10:5, 80:10:10, and 70:10:20 %w/v) nanofibrous scaffolds. * $p < 0.05$; *** $p < 0.001$.

4. Discussion

Functionalization is a strategy which is used in the field of scaffold technology to increase the biocompatibility of a scaffold [44]. In this experiment, P188 was successfully co-electrospun with PCL/gelatin to produce three different functionalized scaffolds (PCL/gelatin/P188 with concentration ratio of 85:10:5, 80:10:10, and 70:10:20 %w/v) with improved cell adhesion and proliferation property. This scaffold has brought together the inherent nanofiber forming ability of PCL, the integrin mediated cell adhesion property of gelatin, and the ability of P188 to revive damaged cells [32,38]. The presence of all the components in the novel nanofibrous scaffold was confirmed by ATR-FTIR analysis.

Many studies in the past have shown the ability of high voltages to stretch the solution and decrease the diameter of the fibers [45–47]. However, no such relationship of a decrease in diameter with an increase in voltage was observed in this study (Table 2). However, the average diameter of more than 50% of the fibrous scaffolds determined using statistical analysis was estimated to be within 200 to 500 nm range (irrespective of their polymer composition), with the highest reproducibility observed for scaffolds electrospun at 22 kV. Another observation with respect to the fiber diameter

is the broader diameter distribution of all the scaffolds except PCL. This is attributed to the fact that the high conductive polymer solutions are unstable in the presence of high voltages, resulting in fibers of varying diameter [45,48]. The conductivity of PCL/gelatin and PCL/gelatin/P188 solutions are significantly higher (around 12 μS) in comparison with the PCL solution (1.9 ± 0.95 μS).

Among the composite fibrous scaffolds, there was a decrease in homogeneity with the decrease in concentration of PCL in the fibers. The PCL/gelatin fibers appeared more homogeneous with fewer polymeric solids when compared to that of PCL/gelatin/P188 composites. Even among PCL/gelatin/P188 composites, the one with the least concentration of PCL (PCL/gelatin/P188, 70:10:20) produced many beads when compared to other two P188 based scaffolds (PCL/gelatin/P188, 85:10:5 and 80:10:10). This could be because of the lowering of viscosity with a decrease in PCL concentration [49]. Similarly, PCL (15%) sample showed a large concentration of beads indicating an instability during electrospinning. A similar observation was made by Ekram et al., who determined that 15% PCL solution produced using 90/10 %v/v acetic acid/formic acid solvent system has low viscosity and low conductivity resulting in electrospinning instabilities [46].

This roughness of the scaffold is known to play a very important role in cell adhesion as a rougher surface provides a larger surface area for cell interaction compared to the smooth surface [50]. AFM analysis of PCL/gelatin/P188 composite with 20% P188 showed the highest mean roughness of 1039 ± 265 nm. Whereas the roughness value obtained for the other two PCL/gelatin/P188 composites with 5% and 10% P188 were 679 ± 33 nm and 683 ± 95 nm, respectively. Although the increase in fiber diameter is known to increase the surface roughness [51–53], the high roughness of the scaffold with 20% P188 was probably due to increasing in P188 concentration. As 20% P188 based composite scaffold electrospun at 22 kv had the lowest average diameter of 306 ± 163 nm when compared to scaffolds with 10% and 5% P188, which had an average diameter of 327 ± 196 nm and 390 ± 158 nm, respectively (Table 2). The mean roughness Ra of PCL/gelatin composite scaffold was 855 ± 11 nm and that of PCL scaffold was 696 ± 134 nm.

The PCL/gelatin/P188 scaffold with 20% P188 also exhibited highest cell proliferation on day two of the cell viability study when compared to the scaffold with 10% and 5% P188. This indicated the initial increase in cell proliferation, with respect to increasing in the concentration of the P188 in the scaffold. However, by day four the percentage fluorescence of the scaffold (PCL/gelatin/P188) with 20% P188 only increased by 17%, whereas those with 5% and 10% P188 showed 29% and 33% increase, respectively. Although the scaffold with 20% P188 had the highest roughness of all, this decrease in cell proliferation could be because of the toxic effect of high P188 concentrations or the beads that are formed due to the low concentration of PCL in the scaffold. As previous studies have observed, beaded scaffolds reduce the surface area to volume ratio, reducing the cell adhesion and growth irrespective of the nanoscale diameter of the fibers [54]. Hence, further studies have to be performed to understand its significance in chemical and physical characteristics of the fiber and its impact on cell proliferation.

The significance of using gelatin in this experiment is attributed to its innate ability to increase biocompatibility of PCL nanofibers [37]. Gelatin possesses many integrin binding sites for efficient cell adhesion and growth [37]. Moreover, gelatin imparts hydrophilicity to the fibers which are known to increase cell adhesion [25,32]. This ability of gelatin to improve biocompatibility can be clearly observed in this experiment. The cell metabolic activity associated with PCL/gelatin increased to a value higher than that associated with PCL by the fourth day of study. Additionally, the higher roughness of PCL/gelatin is likely to be beneficial when compared to PCL nanofibers. Interestingly, the roughness of PCL/gelatin was higher than PCL/gelatin/P188 nanofibers with 5% and 10% P188 concentration, yet the cell proliferation on scaffolds with P188 was significantly higher than PCL/gelatin. This clearly indicates the major role played by P188 to promote cell growth. The least biocompatible PCL nanofibers, on the other hand, exhibited improved cell proliferation when compared to that of control. This is attributed to the nanofibrous architecture of the scaffold which is known to provide the physical cues required for efficient cell adhesion and growth [12,19,20]. In short, the cell proliferation

study clearly indicates that the nanofibrous nature of the scaffold, its roughness, and its composition play a very important role in cell adhesion and proliferation

5. Conclusions

This experiment successfully produced a novel electrospun PCL/gelatin/P188 nanofibrous scaffold with improved cell adhesion and proliferation characteristics (with intestinal epithelial Caco-2 cells), in comparison to PCL, PCL/gelatin fibers and the cell culture plastic. The 3-dimensional (3D) architecture of the scaffold resembles the natural BM. Hence, this novel scaffold may mimic the BM and can be used for the culture of in vitro intestinal models to study drug delivery, nutrition transport, and the entry mechanism of infectious agents and immune cells. The presence of P188 in the fibers considerably improved the cell proliferation when compared to that of PCL/gelatin fibers, but beads were formed with a decrease in PCL concentration as the P188 concentration increased. Therefore, the ratio of PCL and P188 need to be optimised to produce homogeneous and bead-free fibers with desirable cell growth. This study successfully proved that with further optimisation, this novel composite scaffold can efficiently act as a substrate for cell culture and tissue engineering applications.

References

1. Merker, H. Morphology of the basement membrane. *Microsc. Res. Tech.* **1994**, *28*, 95–124. [CrossRef]
2. Morrissey, M.; Sherwood, D. An active role for basement membrane assembly and modification in tissue sculpting. *J. Cell Sci.* **2015**, *128*, 1661–1668. [CrossRef] [PubMed]
3. Fidler, A.; Vanacore, R.; Chetyrkin, S.; Pedchenko, V.; Bhave, G.; Yin, V.; Stothers, C.; Rose, K.; McDonald, W.; Clark, T.; et al. A unique covalent bond in basement membrane is a primordial innovation for tissue evolution. *Proc. Natl. Acad. Sci. USA* **2013**, *111*, 331–336. [CrossRef] [PubMed]
4. Takeuchi, T.; Gonda, T. Distribution of the Pores of Epithelial Basement Membrane in the Rat Small Intestine. *J. Vet. Med Sci.* **2004**, *66*, 695–700. [CrossRef]
5. Mestres, P.; Gomez, L.; Lopez, T.; del Rosario, G.; Lukas, S.; Hartmann, U. The basement membrane of the isolated rat colonic mucosa. A light, electron and atomic force microscopy study. *Ann. Anat.* **2014**, *196*, 108–118. [CrossRef] [PubMed]
6. Candiello, J.; Cole, G.; Halfter, W. Age-dependent changes in the structure, composition and biophysical properties of a human basement membrane. *Matrix Biol.* **2010**, *29*, 402–410. [CrossRef]
7. Van Agtmael, T.; Bruckner-Tuderman, L. Basement membranes and human disease. *Cell Tissue Res.* **2009**, *339*, 167–188. [CrossRef]
8. Kayaselcuk, F.; Serin, E.; Gumurdulu, Y.; Ozer, B.; Tuncer, I.; Boyacioglu, S. Subepithelial basement membrane thickness in patients with normal colonic mucosal appearance in colonoscopy: Results from southern Turkey. *World J. Gastroenterol.* **2004**, *10*, 1056. [CrossRef] [PubMed]
9. Eltboli, O.; Mistry, V.; Barker, B.; Brightling, C. Relationship between blood and bronchial submucosal eosinophilia and reticular basement membrane thickening in chronic obstructive pulmonary disease. *Respirology* **2015**, *20*, 667–670. [CrossRef] [PubMed]

10. Vllasaliu, D.; Fowler, R.; Garnett, M.; Eaton, M.; Stolnik, S. Barrier characteristics of epithelial cultures modelling the airway and intestinal mucosa: A comparison. *Biochem. Biophys. Res. Commun.* **2011**, *415*, 579–585. [CrossRef]

11. Moradi, E.; Vllasaliu, D.; Garnett, M.; Falcone, F.; Stolnik, S. Ligand density and clustering effects on endocytosis of folate modified nanoparticles. *RSC Adv.* **2012**, *2*, 3025. [CrossRef]

12. Vllasaliu, D.; Falcone, F.; Stolnik, S.; Garnett, M. Basement membrane influences intestinal epithelial cell growth and presents a barrier to the movement of macromolecules. *Exp. Cell Res.* **2014**, *323*, 218–231. [CrossRef]

13. Vllasaliu, D.; Thanou, M.; Stolnik, S.; Fowler, R. Recent advances in oral delivery of biologics: Nanomedicine and physical modes of delivery. *Expert Opin. Drug Deliv.* **2018**, *15*, 759–770. [CrossRef]

14. Alfano, M.; Chasens, A.; Masi, C. Autoradiographic study of the penetration of radiolabelled dextrans and inulin through non-keratinized oral mucosain vitro. *J. Periodontal Res.* **1977**, *12*, 368–377. [CrossRef]

15. Fowler, R.; Vllasaliu, D.; Trillo, F.; Garnett, M.; Alexander, C.; Horsley, H.; Smith, B.; Whitcombe, I.; Eaton, M.; Stolnik, S. Nanoparticle Transport in Epithelial Cells: Pathway Switching Through Bioconjugation. *Small* **2013**, *9*, 3282–3294. [CrossRef]

16. Dix, C.; Hassan, I.; Obray, H.; Shah, R.; Wilson, G. The Transport of Vitamin B12 Through Polarized Monolayers of Caco-2 Cells. *Gastroenterology* **1990**, *98*, 1272–1279. [CrossRef]

17. Rescigno, M.; Urbano, M.; Valzasina, B.; Francolini, M.; Rotta, G.; Bonasio, R.; Granucci, F.; Kraehenbuhl, J.; Ricciardi-Castagnoli, P. Dendritic cells express tight junction proteins and penetrate gut epithelial monolayers to sample bacteria. *Nat. Immunol.* **2001**, *2*, 361–367. [CrossRef]

18. Ma, T.; Boivin, M.; Ye, D.; Pedram, A.; Said, H. Mechanism of TNF-α modulation of Caco-2 intestinal epithelial tight junction barrier: Role of myosin light-chain kinase protein expression. *Am. J. Physiol. Gastrointest. Liver Physiol.* **2005**, *288*, G422–G430. [CrossRef]

19. Denning, D.; Roos, W. Elucidating the molecular mechanisms underlying cellular response to biophysical cues using synthetic biology approaches. *Cell Adhes. Migr.* **2016**, *10*, 540–553. [CrossRef]

20. Flemming, R.; Murphy, C.; Abrams, G.; Goodman, S.; Nealey, P. Effects of synthetic micro- and nano-structured surfaces on cell behavior. *Biomaterials* **1999**, *20*, 573–588. [CrossRef]

21. Cruz-Acuña, R.; García, A. Synthetic hydrogels mimicking basement membrane matrices to promote cell-matrix interactions. *Matrix Biol.* **2017**, *57–58*, 324–333. [CrossRef]

22. Kajdič, S.; Vrečer, F.; Kocbek, P. Preparation of poloxamer-based nanofibers for enhanced dissolution of carvedilol. *Eur. J. Pharm. Sci.* **2018**, *117*, 331–340. [CrossRef]

23. Xue, J.; Xie, J.; Liu, W.; Xia, Y. Electrospun Nanofibers: New Concepts, Materials, and Applications. *Acc. Chem. Res.* **2017**, *50*, 1976–1987. [CrossRef]

24. Zhang, Y.; Ouyang, H.; Lim, C.; Ramakrishna, S.; Huang, Z. Electrospinning of gelatin fibers and gelatin/PCL composite fibrous scaffolds. *J. Biomed. Mater. Res.* **2004**, *72B*, 156–165. [CrossRef]

25. Chung, T.; Liu, D.; Wang, S.; Wang, S. Enhancement of the growth of human endothelial cells by surface roughness at nanometer scale. *Biomaterials* **2003**, *24*, 4655–4661. [CrossRef]

26. Engler, A.; Sen, S.; Sweeney, H.; Discher, D. Matrix Elasticity Directs Stem Cell Lineage Specification. *Cell* **2006**, *126*, 677–689. [CrossRef]

27. Goddard, J.; Hotchkiss, J. Polymer surface modification for the attachment of bioactive compounds. *Prog. Polym. Sci.* **2007**, *32*, 698–725. [CrossRef]

28. Jung, H.; Kwak, B.; Yang, H.; Tae, G.; Kim, J.; Shin, K. Attachment of cells to poly(styrene-co-acrylic acid) thin films with various charge densities. *Colloids Surf. A* **2008**, *313–314*, 562–566. [CrossRef]

29. Lee, J.; Jung, H.; Kang, I.; Lee, H. Cell behaviour on polymer surfaces with different functional groups. *Biomaterials* **1994**, *15*, 705–711. [CrossRef]

30. Khatiwala, C.; Peyton, S.; Metzke, M.; Putnam, A. The regulation of osteogenesis by ECM rigidity in MC3T3-E1 cells requires MAPK activation. *J. Cell. Physiol.* **2007**, *211*, 661–672. [CrossRef]

31. Khoda, A. Engineered Tissue Scaffolds with Variational Porous Architecture. *J. Biomech. Eng.* **2010**, *133*, 011001. [CrossRef]

32. Gautam, S.; Dinda, A.; Mishra, N. Fabrication and characterization of PCL/gelatin composite nanofibrous scaffold for tissue engineering applications by electrospinning method. *Mater. Sci. Eng. C* **2013**, *33*, 1228–1235. [CrossRef]

33. Chen, H.; Huang, J.; Yu, J.; Liu, S.; Gu, P. Electrospun chitosan-graft-poly (ε-caprolactone)/poly (ε-caprolactone) cationic nanofibrous mats as potential scaffolds for skin tissue engineering. *Int. J. Biol. Macromol.* **2011**, *48*, 13–19. [CrossRef]

34. Li, W.; Cooper, J.; Mauck, R.; Tuan, R. Fabrication and characterization of six electrospun poly(α-hydroxy ester)-based fibrous scaffolds for tissue engineering applications. *Acta Biomater.* **2006**, *2*, 377–385. [CrossRef]

35. Kim, C.; Khil, M.; Kim, H.; Lee, H.; Jahng, K. An improved hydrophilicity via electrospinning for enhanced cell attachment and proliferation. *J. Biomed. Mater. Res. Part B* **2006**, *78B*, 283–290. [CrossRef]

36. Barnes, C.; Sell, S.; Boland, E.; Simpson, D.; Bowlin, G. Nanofiber technology: Designing the next generation of tissue engineering scaffolds. *Adv. Drug Deliv. Rev.* **2007**, *59*, 1413–1433. [CrossRef]

37. Ghasemi-Mobarakeh, L.; Prabhakaran, M.; Morshed, M.; Nasr-Esfahani, M.; Ramakrishna, S. Electrospun poly(ε-caprolactone)/gelatin nanofibrous scaffolds for nerve tissue engineering. *Biomaterials* **2008**, *29*, 4532–4539. [CrossRef]

38. Kerleta, V. Poloxamer 188 supplemented culture medium increases the vitality of Caco-2 cells after subcultivation and freeze/thaw cycles. *ALTEX* **2010**, *27*, 191–197. [CrossRef]

39. Böttjer, R.; Grothe, T.; Wehlage, D.; Ehrmann, A. Electrospraying poloxamer/(bio-)polymer blends using a needleless electrospinning machine. *J. Text. Fibrous Mater.* **2018**, *1*. [CrossRef]

40. Aytimur, A.; Koçyiğit, S.; Uslu, İ. Synthesis and Characterization of Poly(vinyl alcohol)/Poly(vinyl pyrrolidone)-Iodine Nanofibers with Poloxamer 188 and Chitosan. *Polym. Plast. Technol. Eng.* **2013**, *52*, 661–666. [CrossRef]

41. Denis, P.; Dulnik, J.; Sajkiewicz, P. Electrospinning and Structure of Bicomponent Polycaprolactone/Gelatin Nanofibers Obtained Using Alternative Solvent System. *Int. J. Polym. Mater. Polym. Biomater.* **2014**, *64*, 354–364. [CrossRef]

42. Voytik-Harbin, S.; Brightman, A.; Waisner, B.; Lamar, C.; Badylak, S. Application and evaluation of the alamarblue assay for cell growth and survival of fibroblasts. *In Vitro Cell. Dev. Biol. Anim.* **1998**, *34*, 239–246. [CrossRef]

43. De Oliveira, R.R.L.; Albuquerque, D.A.C.; Leite, F.L.; Yamaji, F.M.; Cruz, T.G.S. *Measurement of the Nanoscale Roughness by Atomic Force Microscopy: Basic Principles and Applications*; INTECH Open Access Publisher: London, UK, 2012.

44. Pham, Q.; Sharma, U.; Mikos, A. Electrospinning of Polymeric Nanofibers for Tissue Engineering Applications: A Review. *Tissue Eng.* **2006**, *12*, 1197–1211. [CrossRef]

45. Bhardwaj, N.; Kundu, S. Electrospinning: A fascinating fiber fabrication technique. *Biotechnol. Adv.* **2010**, *28*, 325–347. [CrossRef]

46. Ekram, B.; Abdel-Hady, B.; El-kady, A.; Amr, S.; Waley, A.; Guirguis, O. Optimum parameters for the production of nano-scale electrospun polycaprolactone to be used as a biomedical material. *Adv. Nat. Sci. Nanosci. Nanotechnol.* **2017**, *8*, 045018. [CrossRef]

47. Yördem, O.; Papila, M.; Menceloğlu, Y. Effects of electrospinning parameters on polyacrylonitrile nanofiber diameter: An investigation by response surface methodology. *Mater. Des.* **2008**, *29*, 34–44. [CrossRef]

48. Hayati, I.; Bailey, A.; Tadros, T. Investigations into the mechanisms of electrohydrodynamic spraying of liquids. *J. Colloid Interface Sci.* **1987**, *117*, 205–221. [CrossRef]

49. Deitzel, J.; Kleinmeyer, J.; Harris, D.; Beck Tan, N. The effect of processing variables on the morphology of electrospun nanofibers and textiles. *Polymer* **2001**, *42*, 261–272. [CrossRef]

50. Cheng, Z.; Teoh, S. Surface modification of ultra thin poly (ε-caprolactone) films using acrylic acid and collagen. *Biomaterials* **2004**, *25*, 1991–2001. [CrossRef]

51. Milleret, V.; Hefti, T.; Hall, H.; Vogel, V.; Eberli, D. Influence of the fiber diameter and surface roughness of electrospun vascular grafts on blood activation. *Acta Biomater.* **2012**, *8*, 4349–4356. [CrossRef]

52. Lim, M.; Sun, T.; Sultana, N. In VitroBiological Evaluation of Electrospun Polycaprolactone/Gelatine Nanofibrous Scaffold for Tissue Engineering. *J. Nanomater.* **2015**, *2015*, 303426. [CrossRef]

53. Hassan, M.; Sultana, N. Characterization, drug loading and antibacterial activity of nanohydroxyapatite/polycaprolactone (nHA/PCL) electrospun membrane. *3 Biotech* **2017**, *7*, 249. [CrossRef]

54. Chen, M.; Patra, P.; Warner, S.; Bhowmick, S. Role of Fiber Diameter in Adhesion and Proliferation of NIH 3T3 Fibroblast on Electrospun Polycaprolactone Scaffolds. *Tissue Eng.* **2007**, *13*, 579–587. [CrossRef]